International Journal of Heat and Mass Transfer 87 (2015) 418–428

Contents lists available at ScienceDirect

International Journal of Heat and Mass Transfer

journal homepage: www.elsevier.com/locate/ijhmt

Temperature-aware time-varying convection over a duty cycle for a given system thermal-topology

M. Fakoor-Pakdaman, Mehran Ahmadi, Majid Bahrami *

Laboratory for Alternative Energy Conversion (LAEC), School of Mechatronic Systems Engineering, Simon Fraser University, Surrey, BC, V3T 0A3, Canada

ARTICLE INFO

Article history:
Received 28 September 2014
Received in revised form 2 April 2015
Accepted 2 April 2015
Available online 24 April 2015

Keywords:
Convection
Dynamic systems
Transient
Experiment
Duty cycle

ABSTRACT

Smart dynamic thermal management (SDTM) is a key enabling technology for optimal design of the emerging transient heat exchangers/heat sinks associated with advanced power electronics and electric machines (APEEM). The cooling systems of APEEM undergo substantial transition as a result of time-varying thermal load over a duty cycle. Optimal design criteria for such dynamic cooling systems should be achieved through addressing internal forced convection under time-dependent heat fluxes. Accordingly, an experimental study is carried out to investigate the thermal characteristics of a laminar fully-developed tube flow under time-varying heat fluxes. Three different transient scenarios are implemented under: (i) step; (ii) sinusoidal; and (iii) square-wave time-varying thermal loads. Based on the transient energy balance, exact closed-form relationships are proposed to predict the coolant bulk temperature over time for the aforementioned scenarios. In addition, based on the obtained experimental data and the methodology presented in Fakoor-Pakdaman et al. (2014), semi-analytical relationships are developed to calculate: (i) tube wall temperature; and (ii) the Nusselt number over the implemented duty cycles. It is shown that there is a 'cut-off' angular frequency for the imposed power beyond which the heat transfer does not feel the fluctuations. The results of this study provide the platform for temperature-aware dynamic cooling solutions based on the instantaneous thermal load over a duty cycle.

1. Introduction

Smart dynamic thermal management (SDTM) is a transformative technology for efficient cooling of advanced power electronics and electric machines (APEEM). APEEM has applications in: (i) emerging cleantech systems, e.g., powertrain and propulsion systems of hybrid/electric/fuel cell vehicles (HE, E, FCV) [1,2]; (ii) sustainable/renewable power generation systems (wind, solar, tidal) [3,4]; (iii) information technology (IT) services (data centers) and telecommunication facilities [5–7]. The thermal load of APEEM substantially varies over a duty cycle; Downing and Kojasoy [8] predicted heat fluxes of $150-200$ [W/cm^2] and pulsed transient heat loads up to 400 [W/cm^2], for the next-generation insulated gate bipolar transistors (IGBTs). The non-uniform and time-varying nature of the heat load is certainly a key challenge in maintaining the temperature of the electronics within its safe and efficient operating limits [9]. As such, the heat exchangers/heat sinks associated with APEEM operate periodically over time and never attain a steady-state condition. Conventionally, cooling systems are conservatively designed for a nominal steady-state or worst-case scenarios, which may not properly represent the thermal behavior of various applications or duty cycles [10]. The state-of-the-art approach is utilizing SDTM to devise a variable-capacity cooling infrastructure for the next-generation APEEM and the associated engineering applications [7]. SDTM responds to thermal conditions by adaptively adjusting the power-consumption profile of APEEMs on the basis of feedback from temperature sensors [5]. Therefore, supervisory thermal control strategies can then be established to minimize energy consumption and safeguard thermal operating conditions [9]. As such, the performance of transient heat exchangers is optimized based on the system "thermal topology", i.e., instantaneous thermal load (heat dissipation) over a duty cycle. For instance, utilizing SDTM in designing the cooling systems of a data center led to significant energy saving, up to 20%, compared to conventionally cooled facility [7]. In addition, in case of the HE/E/FCV, SDTM improves the vehicle overall efficiency, reliability and fuel consumption as well as reducing the weight and carbon foot print of the vehicle [11].

Therefore, there is a pending need for an in-depth understanding of instantaneous thermal characteristics of transient cooling systems over a given duty cycle. However, there are only a few analytical/experimental studies in the open literature on this topic.

* Corresponding author. Tel.: +1 (778) 782 8538; fax: +1 (778) 782 7514.
E-mail addresses: mfakoorp@sfu.ca (M. Fakoor-Pakdaman), mahmadi@sfu.ca (M. Ahmadi), mbahrami@sfu.ca (M. Bahrami).

http://dx.doi.org/10.1016/j.ijheatmasstransfer.2015.04.011
0017-9310/

Nomenclature

a	heat flux amplitude, [W/m^2]
c_p	heat capacity, [J/kg/K]
c_n	coefficients in Eq. (10)
D	tube diameter, [m]
Fo	Fourier number, $= \alpha t/R^2$
h	heat transfer coefficient, [W/m^2/K]
J	Bessel function
k	thermal conductivity, [W/m/K]
L	length, [m]
m	integer number, Eq. (21)
$\dot{m}$	mass flow rate, [kg/s]
Nu_D	local Nusselt number, $= [h(x,t) \times D]/k$
$\overline{Nu}_D$	average Nusselt number, $\frac{1}{L_2}\int_0^{L_2} Nu_D dx$
P	power, [W]
p	period of the imposed power, [s]
Pr	Prandtl number, $= \upsilon/\alpha$
q''	thermal load (heat flux), [W/m^2]
R	tube radius, [m]
r	radial coordinate measured from tube centerline, [m]
Re	Reynolds number, $= UD/\upsilon$
T	temperature, [K]
t	time, [s]
U	velocity, [m/s]
X	dimensionless axial distance, $= 4x/\mathrm{Re}\cdot\mathrm{Pr}\cdot D$
x	axial distance from the entrance of the heated section, [m]

Greek letters

α	thermal diffusivity, [m^2/s]
υ	kinematic viscosity, [m^2/s]
ρ	fluid density, [kg/m^3]
λ_n	Eigenvalues in Eq. (10)
Λ_n	values defined in Eq. (10)
θ	dimensionless temperature, $= \frac{T-T_{in}}{q''_r D/k}$
Ψ	a function defined in Eq. (23)
Υ	a function defined in Eq. (18)
β_n	positive roots of the Bessel function, $J_1(\beta_n) = 0$
ω_1	angular frequency of the sinusoidal heat flux, $= (2\pi R^2)/(p_1\alpha)$
ω_m	dimensionless number characterizing the square-wave heat flux, $= [(2m+1)\pi R^2]/(p_2\alpha)$

Subscripts

1	sinusoidal scenario
2	square-wave scenario
in	inlet
m	mean or bulk value
out	outlet
r	reference value
w	wall

This study is focused on transient internal forced convection as the main representative of the thermal characteristics of dynamic heat exchangers under arbitrary time-varying heat fluxes. In fact, such analyses lead to devising "temperature-aware" cooling solutions based on the system thermal topology (power management) over a given duty cycle. The results of this work will provide a platform for the design, validation and building new smart thermal management systems that can actively and proactively control the cooling systems of APEEMs and similar applications.

1.1. Present literature

Siegel [12–17] pioneered study on transient internal forced-convective heat transfer. Siegel [12] studied laminar forced convection heat transfer for a slug tube-flow where the walls were given a step-change in the heat flux or alternatively a step-change in the temperature. Moreover, the tube wall temperature of channel slug flows for particular types of position/ time-dependent heat fluxes was studied in the literature [17,18]. Most of the pertinent literature was done for laminar slug flow inside a duct. The slug flow approximation reveals the essential physical behavior of the system, while it enables obtaining exact mathematical solution for various boundary conditions. Using this simplification, one can study the effects of various boundary conditions on transient heat transfer without tedious numerical computations [12,15]. Siegel [15] investigated transient laminar forced convection with fully developed velocity profile following a step change in the wall temperature. The obtained solution was much more complex than the response for slug flow which was presented in [12]. It was reported that the results for both slug and fully-developed flows showed the same trends; however, the slug flow under-predicted the tube wall temperature compared to the Poiseuille flow case. Fakoor-Pakdaman et al. [19–22] conducted a series of analytical studies on the thermal characteristics of internal forced convection over a duty cycle to reveal the thermal characteristics of the emerging dynamic convective cooling systems. Such thermal characteristics were obtained for steady slug flow under: (i) dynamic thermal load [19,20]; (ii) dynamic boundary temperature [21]; and (iii) unsteady slug flow under time-varying heat flux [22]. Most literature on this topic is analytical-based; a summary is presented in Table 1.

Table 1
Summary of existing literature on convection under dynamically varying thermal load.

Author	Notes
Siegel [12]	✓ Reported temperature distribution inside a circular tube and between two parallel plates × Limited to step wall heat flux × Limited to slug flow condition × Limited to an analytical-based approach without validation/verification
Siegel [15]	✓ Reported temperature distribution inside a circular tube or between two parallel plates ✓ Covered thermally developing and fully-developed regions ✓ Considered fully-developed velocity profile × Limited to step wall temperature × Nusselt number was defined based on the tube wall and inlet fluid temperature × Limited to an analytical-based approach without validation/verification
Fakoor-Pakdaman et al. [20]	✓ Reported temperature distribution inside a circular tube ✓ Defined the Nusselt number based on the tube wall and fluid bulk temperature × Limited to slug flow condition × The analytical results were only verified numerically
Fakoor-Pakdaman et al. [22]	✓ Reported temperature distribution inside a circular tube ✓ Considered transient velocity profile for the fluid flow × Limited to sinusoidal wall heat flux. × The analytical results were only verified numerically

Our literature review indicates:

- There is no experimental work on transient internal forced-convection over a duty cycle under a time-varying thermal load.
- The presented models in literature for internal flow under dynamic thermal load are limited to slug flow conditions.
- No analytical model exists to predict the thermal characteristics of fully developed flow over a harmonic duty cycles.

Although encountered quite often in practice, the unsteady convection of fully-developed tube flow under time-varying thermal load over a duty cycle has never been addressed in literature; neither experimentally nor theoretically. In other words, the answer to the following question is not clear: "how the thermal characteristics of emerging dynamic cooling systems vary over a duty cycle under time-varying thermal loads (heat fluxes) of the electronics and APEEM?".

An experimental testbed is fabricated to investigate the thermal characteristics of a fully-developed tube flow under different transient scenarios: (i) step; (ii) sinusoidal; and (iii) square-wave heat fluxes. Based on the transient energy balance, exact closed-form relationships are proposed to predict the fluid bulk temperature under the studied transient scenarios (duty cycles). The accuracy of the experimental data is also verified by the obtained results for the fluid bulk temperature. Based on the obtained experimental data and the methodology presented in [13,18], semi-analytical relationships are developed to calculate the: (i) tube wall temperature; and (ii) the Nusselt number over the studied duty cycles. Moreover, easy-to-use relationships are presented as the short-time asymptotes for tube wall temperature and the Nusselt number for the case of step wall heat flux. At early times, $Fo < 0.2$, such asymptotes deviate only slightly from the obtained series solutions as the short-time responses; maximum deviation less than 2%.

2. Real-time data measurement

2.1. Experimental setup

The experimental setup fabricated for this work is shown schematically in Fig. 1. The fluid, distilled water, flows down from an upper level tank and enters the calming section. Adjusting the installed valves, the water level inside the upper-level tank is maintained constant during each experiment to attain the desired values of the constant flow during each experiment.

Following [23], the calming section is long enough so that the fluid becomes hydrodynamically fully-developed at the beginning of the heated section. A straight copper tube with 12.7 ± 0.02 [mm] outer diameter, and 11.07 ± 0.02 [mm] inner diameter is used for the calming and heated sections. The length of the former is $L_1 = 500$ [mm], while the heated section is $L_2 = 1900$ [mm] long. Two flexible heating tapes, STH series Omega, are wrapped around the entire heated section. Four T-type thermocouples are mounted on the heated section at axial positions in [mm] of T1(300), T2(600), T3(1000), and T4(1700) from the beginning of the heated section to measure the wall temperature. In addition, two T-type thermocouples are inserted into the flow at the inlet and outlet of the test section to measure the bulk temperatures of the distilled water. The heating tapes are connected in series, while each is 240 [V] and 890 [W]. To apply the time-dependent power on the heated section, two programmable DC power supplies (Chroma, USA) are linked in a master and slave fashion, and connected to the tape heaters. The maximum possible power is 300 [W]. To reduce heat losses towards the surrounding environment, a thick layer (5 [cm]) of fiber-glass insulating blanket is wrapped around the entire test section including calming and heated sections. After the flow passes through the test section, the flow rate is measured by a precise micro paddlewheel flow meter, FTB300 series Omega. Finally, the fluid returns to the surge tank which is full of ice-water mixture. As a result, the fluid is cooled down, and then is pumped to the main tank at the upper level. All the thermocouples are connected to a data acquisition system composed of an SCXI-1102 module, an SCXI-1303 terminal and an acquisition board; all these components are from National Instrument. The programmable DC power supplies are controlled via standard LabVIEW software (National Instrument), to apply the time-dependent powers. As such, different unsteady thermal duty cycles are attained by applying three different scenarios for the imposed power: (i) step; (ii) sinusoidal; and (iii) square-wave. As such, real-time data are obtained for transient thermal characteristics of the system over such duty cycles; see Section 2.2 for more detail. The accuracy of the measurements and the uncertainties of the derived values are given in Table 2.

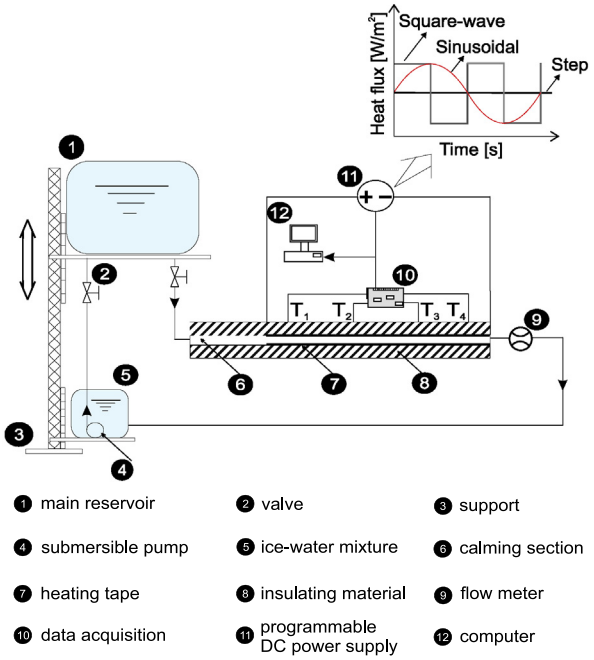

Fig. 1. Schematic view of the fabricated experimental setup.

Table 2
Summary of calculated experimental uncertainties.

Primary measurements		Derived quantities	
Parameter	Uncertainties	Parameter	Uncertainties (%)
$\dot{m}$	6%	Re	7.6
P [W]	3%	h [W/m^2/K]	8.1
$T(T_{in}, T_{out}, T_m)$	0.5[°C]	Nu	8.3

2.2. Data processing

In most Siegel works [13,18], the transient thermal behavior of a system is evaluated based on the dimensionless wall heat flux considering the difference between the local tube wall and the initial fluid temperature. We are of the opinion that an alternative definition of the local Nusselt number has a more 'physical' meaning, i.e., based on the local difference between the channel wall and the fluid bulk temperature at each axial location; this is consistent with [24,25]. It should be emphasized that the definition of the Nusselt number is an arbitrary choice and will not alter the final results. As such, the overall transient convective heat transfer coefficient is defined as follows:

$$\overline{h}(L_2,t)=\frac{q''(t)}{\overline{T_w}(t)-\overline{T_m}(t)} \tag{1}$$

where $q''(t)$ is the applied time-dependent heat flux, $\overline{T_w}(t)$ is the average tube wall temperature, and $\overline{T_m}(t)$ is the arithmetic average of inlet and outlet fluid bulk temperatures. Therefore, the definitions of different parameters in Eq. (1) are given below:

$$\overline{T_w}(t)=\frac{1}{4}\sum_{i=1}^{4}T_i(t) \tag{2}$$

$$\overline{T_m}(t)=\frac{T_{in}(t)+T_{out}(t)}{2} \tag{3}$$

$$q''(t)=\frac{P(t)}{\pi DL_2} \tag{4}$$

where T_{in} and T_{out} are the inlet and outlet fluid temperatures, respectively. Moreover, $P(t)$ is the applied transient power and L_2 is the length of the heated section. The overall Nusselt number is also obtained by the following relationship.

$$\overline{Nu}_D(L_2,t)=\frac{\overline{h}(L_2,t)\times D}{k} \tag{5}$$

where, D and k are the tube diameter and fluid thermal conductivity, respectively. The thermo-physical properties of the distilled water used in this study are determined at the arithmetic average temperature, $\overline{T_m}(t)$, from [23].

3. Model development

In this section, it is intended to present closed-form solutions for the thermal characteristics of laminar tube flow under the transient scenarios, i.e., (i) step; (ii) sinusoidal; and (iii) square-wave heat fluxes. Following Siegel [13] and Fakoor-Pakdaman et al. [20,22], closed-form relationships are obtained to calculate: (i) tube wall temperature; (ii) fluid bulk temperature; and (iii) the Nusselt number, for the above-mentioned time-dependent heat fluxes.

The methodology presented in [13] proceeds as follows: consider a position x in the channel through which the fluid is flowing with average velocity U. A fluid element starting from the entrance of the channel will require time duration $t=x/U$ to reach the x location. In the region where $x/U\geqslant t$, i.e., short-time response, there is no penetration of the fluid which was at the entrance when the transient began. Therefore, the short-time response corresponds to pure transient heat conduction, and the effect of heat convection is zero. However, for the region $x/U\leqslant t$, the heat transfer process occurs via the fluid that entered the channel after the transient was initiated. This forms the long-time response which is equal to short time response at the transition time, i.e., $t=x/U$. Therefore, the solution composed of two parts that should be considered separately: (i) short-time and (ii) long-time responses. More detail regarding the short- and long-time responses were presented elsewhere [19–22].

3.1. Step power (heat flux)

For this scenario, the imposed heat flux is considered in the following form:

$$q''(t)=\begin{cases}0 & t<0\\ q_r''=\text{const.} & t\geqslant 0\end{cases} \tag{6}$$

where q_r'' (offset), is a constant value over the entire heating period. When a tube flow is suddenly subjected to a step heat flux, the short-time response for the tube wall temperature is obtained as follows [12]:

$$\theta_w=Fo+\frac{1}{8}-\sum_{n=1}^{\infty}\frac{e^{-\beta_n^2Fo}}{\beta_n^2} \tag{7}$$

where β_n are the positive roots of $J_1(\beta)=0$, and $J_1(\beta)$ are the first-order Bessel functions of the first kind, respectively. In addition, θ_w and Fo are the dimensionless wall temperature and dimensionless time, respectively. Such dimensionless numbers are defined as follows:

$$\theta_w=\frac{T_w-T_{in}}{q_r''D/k};\quad Fo=\frac{\alpha t}{R^2} \tag{8}$$

where T_w, T_{in}, k, and α are tube wall temperature, inlet temperature, fluid thermal conductivity, and diffusivity, respectively. It should be noted that when $Fo\to 0$, Fakoor-Pakdaman and Bahrami [26], presented a compact easy-to-use relationship for Eq. (7) as the short-time asymptote for the tube wall temperature. For $Fo<0.2$, the maximum deviation between the series solution, Eq. (7), and the compact model, Eq. (9), is less than 2%.

$$\theta_{w,Fo\to 0}=\left(\sqrt{\frac{\pi}{Fo}}-\frac{\pi}{4}\right)^{-1} \tag{9}$$

In addition, the long-time asymptote can be obtained by a well-known Graetz solution [25] as given below:

$$\theta_w=X+\frac{11}{48}+\frac{1}{2}\sum_{n=1}^{\infty}C_n\Lambda_n\exp\left(-\frac{\lambda_n^2X}{2}\right) \tag{10}$$

where $X=\frac{4x/D}{\mathrm{Re}\cdot\mathrm{Pr}}$ is the dimensionless axial location. Besides, the values of λ_n and $C_n\Lambda_n$ are tabulated in [25]. In addition, the fluid bulk temperature can be obtained by performing a heat balance on an infinitesimal differential control volume of the flow;

$$\dot{m}c_pT_m+q''(\pi D)dx-\left(\dot{m}c_pT_m+\dot{m}c_p\frac{\partial T_m}{\partial x}dx\right)=\rho c_p\left(\frac{\pi D^2}{4}\right)\frac{\partial T_m}{\partial t}dx \tag{11}$$

where $\dot{m}$ is the fluid mass flow rate, c_p and T_m are specific heat and fluid bulk temperature, respectively. The dimensionless form of Eq. (11) is:

$$\frac{q''(X,Fo)}{q_r''}=\frac{\partial\theta_m}{\partial Fo}+\frac{\partial\theta_m}{\partial X} \tag{12}$$

where q_r'' is the offset around which the imposed heat flux fluctuates. Eq. (12) is a first-order partial differential equation which can be solved by the method of characteristics [27]. The short- and long-time asymptotes for the fluid bulk temperature for the case of step heat flux are [26];

$$\theta_m=\begin{cases}Fo & \text{short}-\text{time asymptote}\\ X & \text{Long}-\text{time asymptote}\end{cases} \tag{13}$$

Following Fakoor-Pakdaman and Bahrami [26], the short-time asymptote for the average Nusselt number under a step heat flux can be calculated by a compact relationship, Eq. (14).

$$Nu_D(t)_{Fo\to 0}=\frac{h(t)\times D}{k}=\sqrt{\frac{\pi}{Fo}} \tag{14}$$

In addition, the following well-known Shah equation [28] is used as the long-time asymptote for the average Nusselt number of laminar flow under constant wall heat flux.

$$Nu_{0-x,D}=\begin{cases}1.953X^{-1/3} & \text{for}\quad X\leqslant 0.03\\ 4.364+\frac{0.0722}{X} & \text{for}\quad X>0.03\end{cases} \tag{15}$$

3.2. Sinusoidal power (heat flux)

For this case, the applied heat flux is considered in the following form.

$$q'' = q''_r + a \times \sin\left(\frac{2\pi}{p_1}t\right) \tag{16}$$

where, q''_r [W/m^2], a [W/m^2], and p_1 [s] are the offset, amplitude, and period of the imposed heat flux. The dimensionless form of Eq. (16) is:

$$\frac{q''}{q''_r} = 1 + \left(\frac{a}{q''_r}\right) \times \sin(\omega_1 Fo) \tag{17}$$

where, $\omega_1 = \frac{2\pi R^2}{p_1 \alpha}$ is the dimensionless angular frequency of the imposed heat flux, and R [m] is the tube radius. Substituting Eq. (17) into Eq. (12), closed-form relationships are obtained for the short- and long-time responses for fluid bulk temperature, see Eqs. (18.a) and (18.b). In addition, following the methodology presented in [20], semi-analytical relationships are proposed to predict the tube wall temperature, Eqs. (19.a) and (19.b). Table 3 presents a summary of the results obtained for short- and long-time responses of tube wall and fluid bulk temperatures under a sinusoidal heat flux. It should be noted that C_1 in Eqs. (19.a) and (19.b), is a coefficient which depends on the velocity profile of the fluid inside the tube. It takes the value of unity for slug flow inside the duct, i.e., uniform velocity across the tube, see [20]. For a parabolic velocity profile (poiseuille flow), the value of such coefficient is obtained in this study empirically, and will be discussed in Section 4, where the functions $\Upsilon_{1,n}$ and $\Upsilon_{2,n}$ are defined as:

$$\begin{cases} \Upsilon_{1,n} = \frac{e^{-\beta_n^2 Fo}}{\beta_n^2} + \frac{\omega_1 (a/q''_r)}{\omega_1^2 + \beta_n^4} \times \left[\cos(\omega_1 Fo) - \frac{\beta_n^2}{\omega_1} \times \sin(\omega_1 Fo) - e^{-\beta_n^2 Fo}\right] \\ \Upsilon_{2,n} = \frac{e^{-\beta_n^2 X}}{\beta_n^2} + \frac{\omega_1 (a/q''_r)}{\omega_1^2 + \beta_n^4} \times \left\{ \cos(\omega_1 Fo) - \frac{\beta_n^2}{\omega_1} \times \sin(\omega_1 Fo) + e^{-\beta_n^2 X} \times \begin{Bmatrix} \frac{\beta_n^2}{\omega_1} \times \sin[\omega_1 (Fo - X)] - \\ \cos[\omega_1 (Fo - X)] \end{Bmatrix} \right\} \end{cases} \tag{18}$$

In addition, the short- and long-time local Nusselt numbers can be calculated by the following relationship:

$$Nu_D(x,t) = \frac{q'' D/k}{T_w - T_m} = C_2 \left[\frac{1 + \sin(\omega_1 Fo)}{\theta_w - \theta_m}\right] \tag{19}$$

Again C_2 is a coefficient which takes a value of unity for slug flow inside the duct [20]. The value of such coefficient for a parabolic velocity in this study is obtained empirically, and discussed in Section 4 of this study. Accordingly, the average Nusselt number over the entire length of the heated section, L_2, is calculated as follows:

$$\overline{Nu_D}(L_2,t) = \frac{1}{L_2}\int_0^{L_2} Nu_D dx \tag{20}$$

3.3. Square-wave power (heat flux)

The Fourier series for a square-wave heat flux with offset q''_r, amplitude a, and period p_2 is, [29]:

$$q'' = q''_r + a \times \sum_{m=0,1,2}^{\infty} \frac{1}{2m+1} \sin\left[\frac{(2m+1)\pi}{p_2}t\right] \tag{21}$$

The dimensionless form of Eq. (21) is:

$$\frac{q''}{q''_r} = 1 + \left(\frac{a}{q''_r}\right) \times \sum_{m=0,1,2}^{\infty} \frac{1}{2m+1} \sin(\omega_m Fo) \tag{22}$$

where $\omega_m = \frac{(2m+1)\pi R^2}{p_2 \alpha}$ is a dimensionless number which characterizes the behavior of the square-wave heat flux. Substituting Eq. (22) into Eq. (12), closed-form relationships are obtained for the short- and long-time responses for fluid bulk temperature, see Eqs. (25.a) and (25.b). In addition, following the methodology presented in [20], semi-analytical relationships are proposed to predict the tube wall temperature, Eqs. (26.a) and (26.b). Table 4 presents a summary of the results obtained for short- and long-time responses of tube wall and fluid bulk temperatures under a square-wave heat flux.

Table 3
Tube wall and fluid bulk temperatures for transient scenario II: sinusoidal heat flux, [20].

Short-time response, $X \leqslant Fo$	Long-time response, $X \geqslant Fo$
Fluid bulk temperature, $\theta_m = \frac{T_m - T_{in}}{q''_r D/k}$	
$= Fo + \frac{(a/q''_r)}{\omega_1}[1 - \cos(\omega_1 Fo)]$ (18.a)	$= X + \frac{(a/q''_r)}{\omega_1}\{\cos[\omega_1(Fo - X)] - \cos(\omega_1 Fo)\}$ (18.b)
Tube wall temperature, $\theta_w = \frac{T_w - T_{in}}{q''_r D/k}$	
$= C_1 \begin{Bmatrix} Fo + \frac{(a/q''_r)}{\omega_1} \times [1 - \cos(\omega_1 Fo)] \\ + \frac{1}{8} - \sum_{n=1}^{\infty} \Upsilon_{1,n} \end{Bmatrix}$ (19.a)	$= C_1 \begin{Bmatrix} X + \frac{(a/q''_r)}{\omega_1} \times \begin{Bmatrix} \cos[\omega_1(Fo - X)] \\ -\cos(\omega_1 Fo) \end{Bmatrix} \\ + \frac{1}{8} - \sum_{n=1}^{\infty} \Upsilon_{2,n} \end{Bmatrix}$ (19.b)

Table 4
Tube wall and fluid bulk temperatures for transient scenario III: square-wave heat flux, Ref. [20].

Short-time response, $X \leqslant Fo$	Long-time response, $X \geqslant Fo$
Fluid bulk temperature, $\theta_m = \frac{T_m - T_{in}}{q''_r D/k}$	
$= X + \left(\frac{a}{q''_r}\right) \times \sum_{m=0,1,2}^{\infty} \frac{1}{\omega_m(2m+1)} \begin{Bmatrix} \cos[\omega_m(Fo - X)] \\ -\cos(\omega_m Fo) \end{Bmatrix}$ (25.a)	$= X + \left(\frac{a}{q''_r}\right) \times \sum_{m=0,1,2}^{\infty} \frac{1}{\omega_m(2m+1)} \begin{Bmatrix} \cos[\omega_m(Fo - X)] \\ -\cos(\omega_m Fo) \end{Bmatrix}$ (25.b)
Tube wall temperature, $\theta_w = \frac{T_w - T_{in}}{q''_r D/k}$	
$= C_2 \begin{Bmatrix} Fo + \\ (a/q''_r) \times \sum_{m=0,1,2}^{\infty} \frac{1}{\omega_m(2m+1)} \times \begin{bmatrix} 1 \\ -\cos(\omega_m Fo) \end{bmatrix} \\ + \frac{1}{8} - \sum_{n=1}^{\infty} \Psi_{1,n} \end{Bmatrix}$ (26.a)	$= C_2 \begin{Bmatrix} X + \\ \frac{(a/q''_r)}{\omega_m} \times \sum_{m=0,1,2}^{\infty} \frac{1}{\omega_m(2m+1)} \times \begin{Bmatrix} \cos[\omega_m(Fo - X)] \\ -\cos(\omega_m Fo) \end{Bmatrix} \\ + \frac{1}{8} - \sum_{n=1}^{\infty} \Psi_{2,n} \end{Bmatrix}$ (26.b)

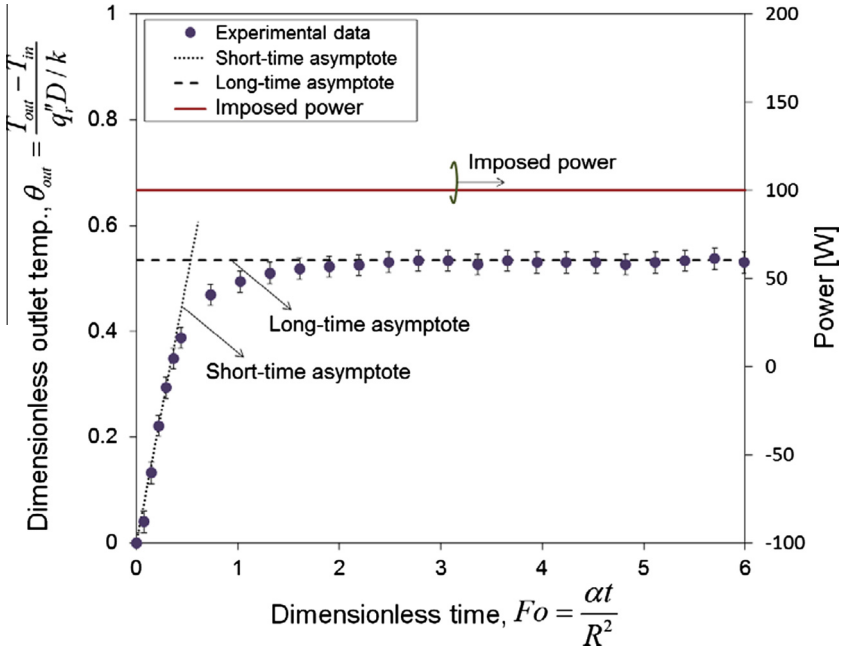

Fig. 2. Short- and long-time asymptotes for outlet fluid bulk-temperature and comparison with experimental data for the step power. ($\dot{m} = 3.3 \pm 0.198$ [gr/s]).

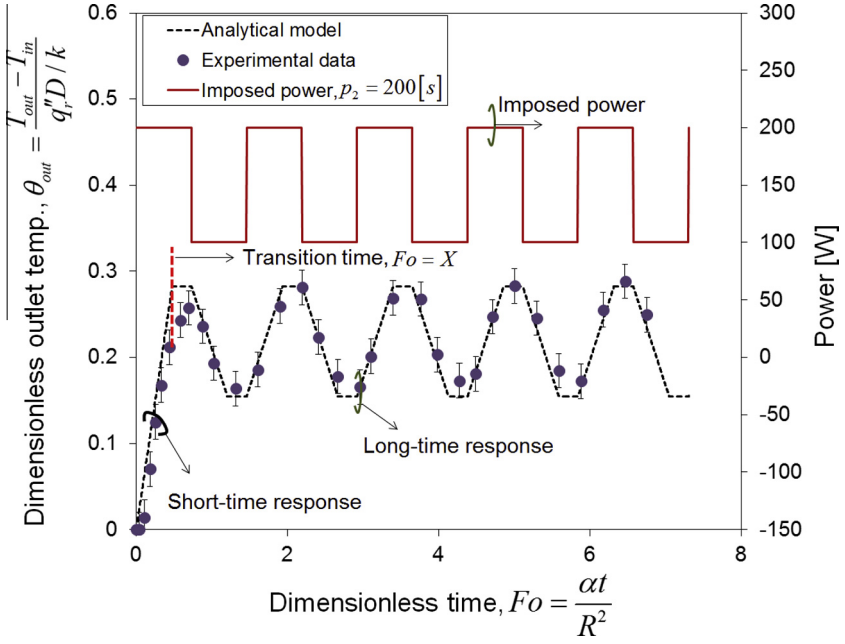

Fig. 3. Short- and long-time responses for outlet fluid bulk temperature and comparison with experimental data for the square-wave power. ($\dot{m} = 3.6 \pm 0.216$ [gr/s]).

The functions $\Psi_{1,n}$ and $\Psi_{2,n}$ are defined as:

$$\begin{cases} \Psi_{1,n} = \frac{e^{-\beta_n^2 Fo}}{\beta_n^2} + (a/q''_r) \times \sum_{m=0,1,2}^{\infty} \frac{\omega_m}{(2m+1)(\omega_m^2+\beta_n^4)} \times \left[\cos(\omega_m Fo) - \frac{\beta_n^2}{\omega_m} \times \sin(\omega_m Fo) - e^{-\beta_n^2 Fo}\right] \\ \Psi_{2,n} = \frac{e^{-\beta_n^2 X}}{\beta_n^2} + (a/q''_r) \times \sum_{m=0,1,2}^{\infty} \frac{\omega_m}{(2m+1)(\omega_m^2+\beta_n^4)} \times \left\{ \begin{array}{l} \cos(\omega_m Fo) - \frac{\beta_n^2}{\omega_m} \times \sin(\omega_m Fo) + \\ e^{-\beta_n^2 X} \times \left\{ \begin{array}{l} \frac{\beta_n^2}{\omega_m} \times \sin[\omega_m (Fo - X)] - \\ \cos[\omega_m (Fo - X)] \end{array} \right. \end{array} \right. \end{cases} \quad (23)$$

In addition, the short- and long-time local Nusselt numbers can be obtained by the following relationship:

$$Nu_D(x,t) = \frac{q'' D/k}{T_w - T_m} = C_2 \left[\frac{1 + \left(\frac{a}{q''_r}\right) \times \sum_{m=0,1,2}^{\infty} \frac{1}{2m+1} \sin(\omega_m Fo)}{\theta_w - \theta_m} \right] \quad (24)$$

Similar to Section 3.2, the average Nusselt number over the entire length of the heated section is:

$$\overline{Nu_D}(L_2,t) = \frac{1}{L_2} \int_0^{L_2} Nu_D dx \quad (25)$$

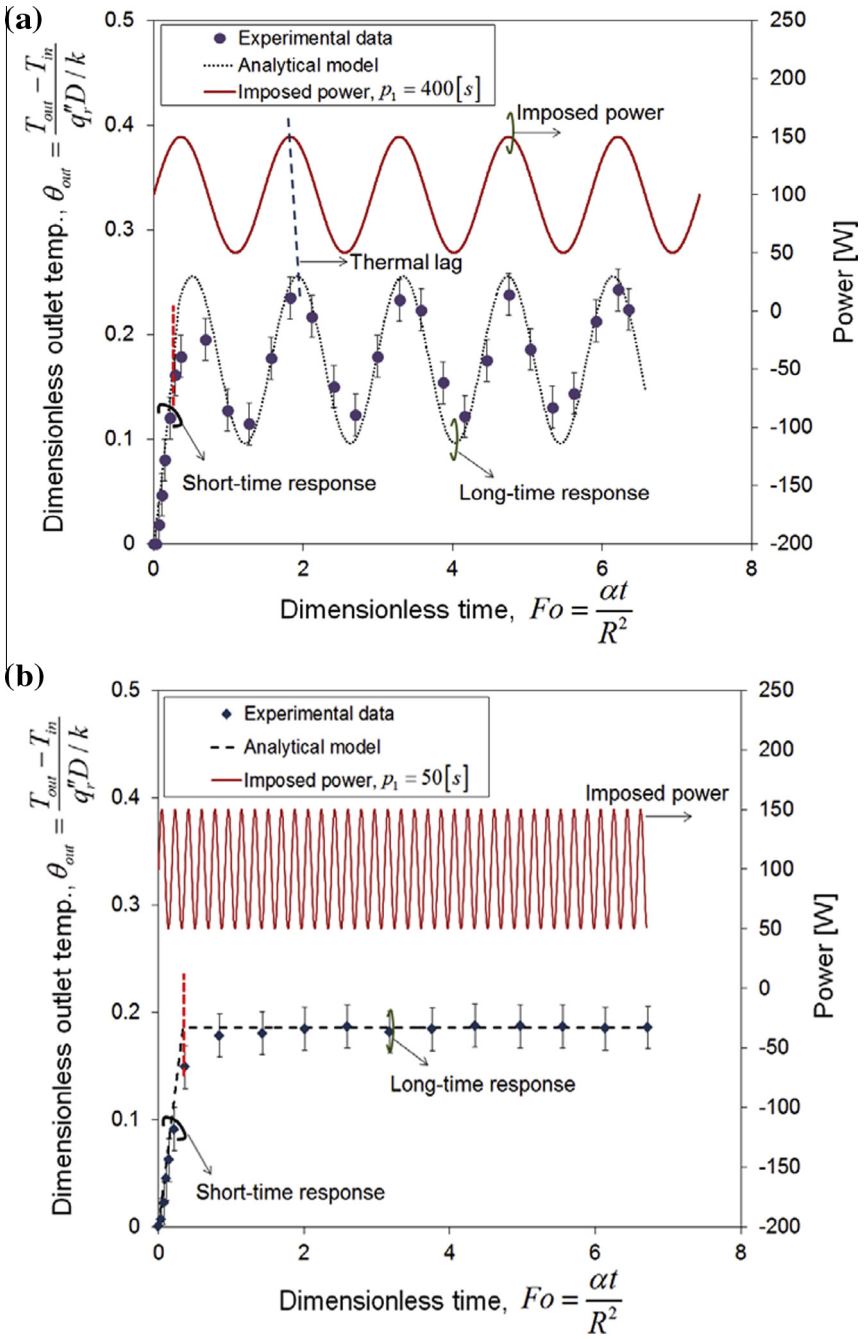

Fig. 4. Short- and long-time responses for outlet temperature and comparison with experimental data for sinusoidal power with different periods: (a) $p_1 = 400$ [s] and (b) $p_1 = 50$ [s]. ($\dot{m} = 3.6 \pm 0.216$ [gr/s]).

4. Results and discussion

4.1. Validation tests/outlet fluid bulk-temperature

Fig. 2 shows the dimensionless short- and long-time asymptotes, Eq. (13), for the outlet fluid bulk-temperature against the dimensionless time (Fourier number) for a step power. The exact analytical results are also compared with the obtained experimental data in Fig. 2.

The following highlights the trends in Fig. 2:

- There is an excellent agreement between the exact analytical solutions and the obtained experimental data. The maximum relative difference between the derived asymptotes and the experimental data is less than 8%.
- The good agreement between the analytical results and the experimental data verifies the accuracy of the experimental setup and the measuring instruments.
- As the heating is applied, the outlet fluid bulk-temperature increases to reach the steady-state value at the long-time asymptote.
- The experimental data show a smooth transition between the short- and long-time responses.

Fig. 3 depicts the variations of dimensionless outlet fluid bulk-temperature against the Fourier number for a square-wave power. The exact analytical results are also compared with the obtained experimental data in Fig. 3. The following conclusions can be drawn from Fig. 3:

- There is a good agreement between the analytical results and the obtained experimental data; the maximum relative difference less than 12%.
- The good agreement between the analytical results and the experimental data verifies the accuracy of the experimental setup and the measuring instruments.
- As the heating is applied, the temperature of the fluid rises to show steady oscillatory behavior after the transition time, $X = Fo$. This time is demarcated on Fig. 3 by a vertical dash line.
- There is an initial transient period, which can be considered as pure conduction, i.e., the short-time response for $X \geqslant Fo$. However, as pointed out earlier, each axial position shows steady oscillatory behavior for $X < Fo$ at the long-time response.
- There is a slight discrepancy between the analytical results and experimental data around the transition time. Referring to [12,20], this happens as a result of the limitations of the mathematical method "method of characteristics" that is used in [20] to solve the energy equation. Such mathematical method predicts an abrupt transition from short- to long-time responses while experimental data show a smooth transition.
- As expected the fluid temperature fluctuates with time in case of a square-wave heat flux. For a step heat flux, the solution does not fluctuate over time. The temperature fluctuates with the period of the imposed heat flux.

4.2. Cut-off angular frequency

Fig. 4 shows the dimensionless outlet fluid bulk-temperature versus the Fourier number under a sinusoidal power. To investigate the effects of the angular frequency of the applied heat flux on the coolant behavior, "slow" and "fast" functions are taken into account for the imposed power. Fig. 4a shows a "slow" transient scenario where the angular frequency of the applied power is $p_1 = 400$ [s], while the corresponding value in the "fast" case in Fig. 4b is $p_1 = 50$ [s]. The following highlights the trends in Fig. 4:

- There is a shift between the peaks of the applied power and the outlet fluid bulk-temperature. This shows a "thermal lag" (inertia) of the fluid flow. This thermal lag is attributed to the fluid thermal inertia.
- When a sinusoidal cyclic heat flux with high angular frequency is imposed on the flow, the fluid does not follow the details of the heat flux behavior. Therefore, for very high angular frequencies, the fluid flow acts as if the imposed heat flux is constant at "the average value" associated with zero frequency for the sinusoidal heat flux.
- For high angular frequencies, i.e., $p \to 0$ or $\omega \to \infty$, the fluid flow response yields that of a step heat flux. This is called the "cut-off" pulsation frequency.
- Dimensionless cut-off angular frequency: defined in this study as the angular frequency beyond which the fluid response lies within $\pm 5\%$ of that of step heat flux. As such, following [22], for a fully developed tube flow subjected to a sinusoidal wall heat flux, $\omega_1 = \frac{2\pi R^2}{p_1 \alpha} = 15\pi$ is the cut-off angular frequency.
- The dimensionless cut-off frequency is a function of heat flux period, p_1 [s], tube radius, R [m], and fluid thermal diffusivity, α [$\frac{m^2}{s}$].
- Irrespective of Fo number, the amplitude of the dimensionless fluid bulk-temperature decreases remarkably as the angular frequency increases. As mentioned earlier, this happens due to the fact that for high angular frequencies the fluid flow response approaches to that of the step heat flux.

4.3. Tube wall temperature

Fig. 5 shows variations of short- and long-time asymptotes for tube wall temperature, Eqs. (7) and (10), against the dimensionless time (Fourier number). A comparison is also made in Fig. 6 between the presented asymptotes, Eqs. (7) and (10), and the obtained experimental data. Step heat flux, Eq. (6), is imposed on the tube wall and the experimental data are reported for the thermocouples T_1 and T_4 which are corresponding to axial locations $X = 0.15$ and 0.4, respectively. The trends for other axial locations are similar.

The following conclusions can be drawn from Fig. 5:

- As heating is applied, the wall temperature rises and then levels out at a steady state value, i.e., long-time asymptote.

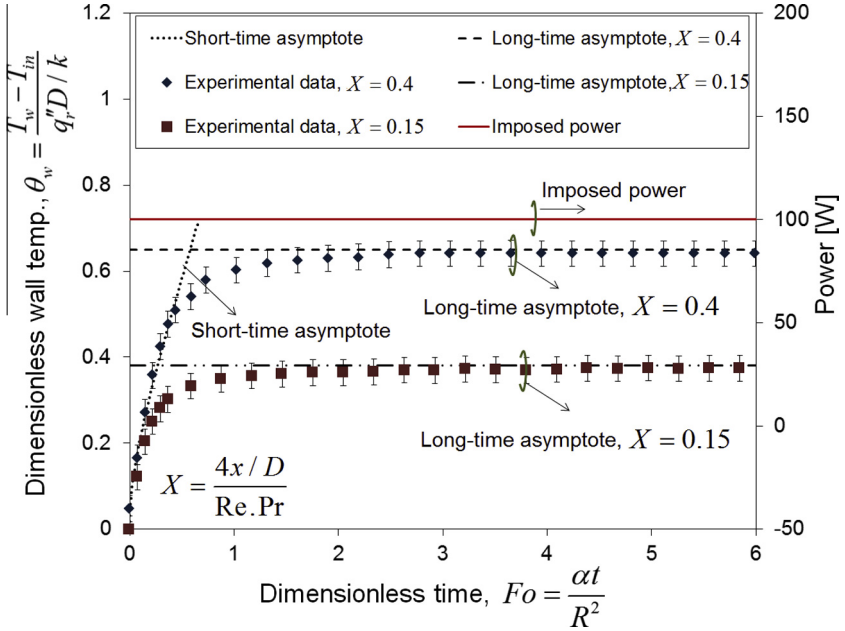

Fig. 5. Short- and long-time asymptotes for tube wall temperature and comparison with experimental data for the step power. ($\dot{m} = 3.3 \pm 0.198$ [gr/s]).

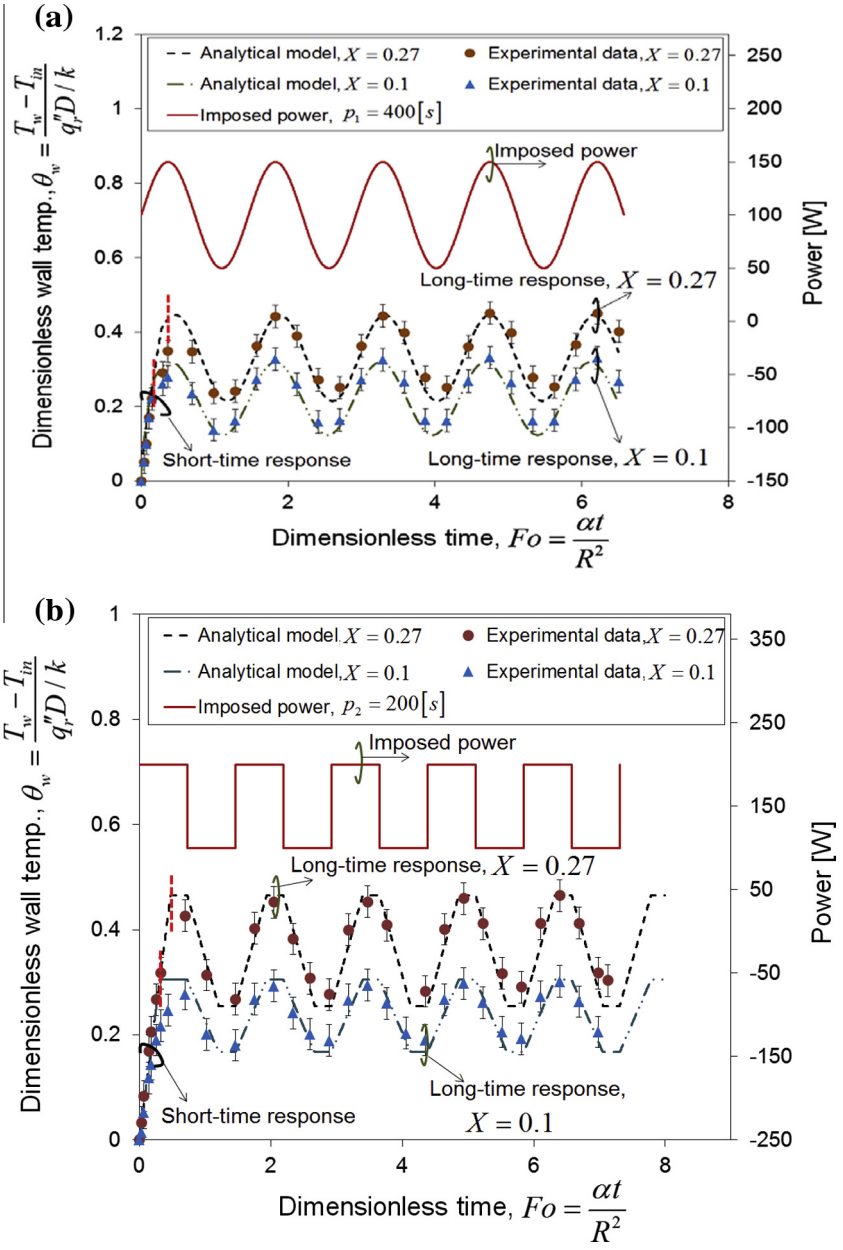

Fig. 6. Short- and long-time responses for tube wall temperature and comparison with experimental data for: (a) sinusoidal and (b) square-wave power. ($\dot{m} = 3.6 \pm 0.216$ [gr/s]).

- There is a good agreement between the experimental data and the short- and long-time asymptotes, Eqs. (9) and (10); maximum relative difference less than 9.2%.
- The obtained experimental data show a smooth transition between the short- and long-time asymptote.
- Around the transition time, the experimental data branch off from the short-time asymptote and plateau out at the long-time asymptote, Eq. (10).

Fig. 6 depicts the variations of closed-form solutions and experimental results for tube wall temperature over the dimensionless time (Fourier number) for: (a) sinusoidal power, Eqs. (19.a) and (19.b); and (b) square-wave power, Eq. (26.a) and (26.b). The experimental data are reported for the thermocouples T_1 and T_3 which are corresponding to $X = 0.1$ and 0.27, respectively. The trends for other axial locations are similar. The following highlights the trends in Fig. 6:

- There is an initial transient period of pure conduction, i.e., short-time response, during which all of the curves follow along the same line, $X \geqslant Fo$.
- When $Fo = X$, each curve moves away from the common line, i. e., pure conduction response and adjusts towards a steady oscillatory behavior at long-time response. The transition time for the axial locations considered in Fig. 6, are indicated by vertical dash lines.
- The wall temperatures become higher for larger X values, as expected, because of the increase in the fluid bulk temperature in the axial direction.
- As mentioned before, the value of C_1 is unity for slug flow, while it should be obtained empirically for other velocity profiles. Based on the obtained experimental data, the value of C_1 is considered equal to 1.7; in mathematical notation, $C_1 = 1.7$. As such, there is an excellent agreement between the closed-form relationships Eqs. (16) and (22), and the experimental data over the short-and long-time responses.

- There is a small discrepancy between the experimental data and analytical results around the transition time, $X = Fo$. As mentioned before, this is attributed to the limitations of the mathematical approach "method of characteristics" that cannot predict the results around the transition time accurately. The maximum relative difference between the present analytical model and the experimental data is less than 10.1%.

4.4. Nusselt number

Variations of the average Nusselt number against the Fourier number for a step power are depicted in Fig. 7. Short- and long-time responses are shown in Fig. 7, and compared with the obtained experimental data. Moreover, a relationship is proposed as an all-time Nusselt number based on the blending technique [30]. The following can be concluded from Fig. 7:

- There is a good agreement between the short-time asymptote, Eq. (14), and the obtained experimental data at early times, $Fo \to 0$.
- Around the transition time, the experimental data branch off from the short-time asymptote and adjust towards the long-time asymptote.
- Based on the blending technique [31], the following relationship is proposed as an all-time model for the average Nusselt number under a step heat flux.

$$\overline{Nu}_D(t,x) = \left\{ [(Nu_D(t)_{Fo\to 0})]^3 + [Nu_{0-x,D}]^3 \right\}^{(1/3)} \tag{26}$$

where $Nu_D(t)$ and $Nu_{0-x,D}$ are the short- and long-time asymptotes, Eqs. (14) and (15). In addition, $\overline{Nu}_D(t,x)$ is the all-time model presented for the average Nusselt number for a step power.

- The maximum relative difference between the proposed all-time model and the experimental data is less than 7%.

Fig. 8 shows the variations of the average Nusselt number against the Fourier number for the sinusoidal imposed heat flux. Different periods are considered for the imposed power and the semi-analytical results are compared with obtained experimental data. Regarding Fig. 8, the conventional "quasi-steady" model is a simplified model which assumes that the convective heat transfer coefficient is constant, equal to the fully developed condition in the channel [13]. It should be noted that based on the obtained experimental data, the value of the coefficient C_2 is considered equal to

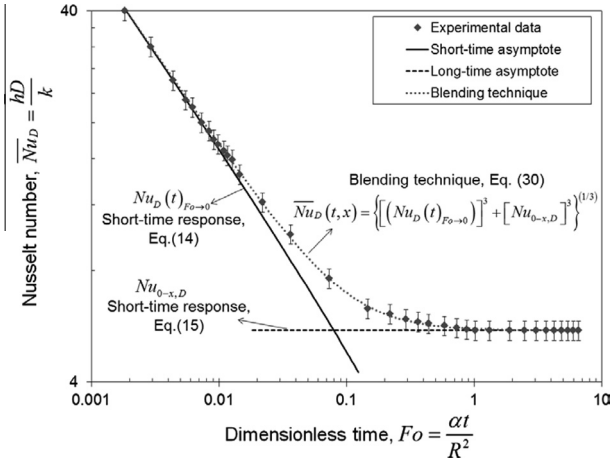

Fig. 7. Short- and long-time responses as well as the proposed all-time model for the average Nusselt number, and comparison with the obtained experimental data for the step power. ($\dot{m} = 3.3 \pm 0.198$ [gr/s]).

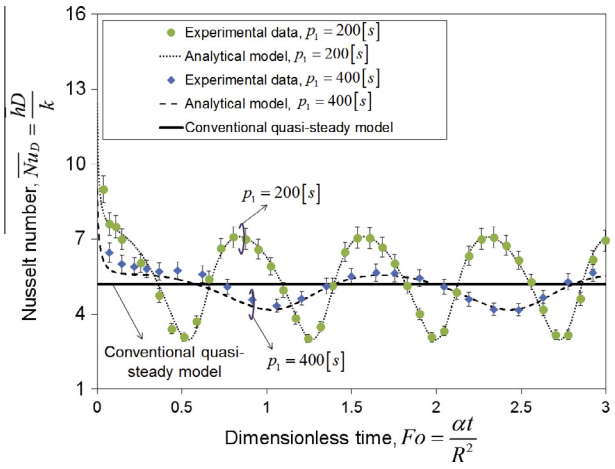

Fig. 8. All-time Nusselt number for sinusoidal transient scenario with different periods of $p_1 = 200$ [s] and $p_1 = 400$ [s], and comparison with quasi-steady model and the obtained experimental data. ($\dot{m} = 3.6 \pm 0.216$ [gr/s]).

0.54. Such value minimizes the difference between the experimental and semi-analytical results; maximum relative difference less than 10%. The following highlights the trends in Fig. 8.

- The values of the average Nusselt number vary significantly with the angular frequency of the imposed heat flux, while the conventional models, e.g., quasi-steady model fail to predict such variations of the Nusselt number with time.
- The Nusselt number oscillates with the angular frequency of the imposed heat flux.
- Regardless of the angular frequency, at very initial transient period, the Nusselt number is much higher than that of the long-time response.
- The fluctuations of the transient Nusselt number occur somewhat around the fully-developed steady-state value. Considering the slug flow inside a circular tube, the value of the fully-developed Nusselt number for the steady-state condition is: $Nu_D = 4.36$ as predicted by the quasi-steady model [25].

6. Conclusion

An experimental study is carried out to investigate the thermal characteristics of a fully-developed tube flow under time-varying heat fluxes. Three different scenarios are considered for the applied time-dependent heat fluxes: (i) step; (ii) sinusoidal; and (iii) square-wave. Exact closed-form relationships are proposed to find the fluid bulk temperature for the implemented scenarios. As such, the accuracy of the experimental data and the measuring instruments are verified. Semi-analytical relationships are proposed to predict; (i) tube wall temperature and (ii) the Nusselt number for all the implemented scenarios. The question "how the thermal characteristics of the dynamic cooling systems vary over a duty cycle" is answered here as follows: The imposed heat flux (thermal load) is the dominant parameter that characterizes the thermal behavior of a cooling system. As such;

- The temperature and the Nusselt number fluctuate with the period of the applied thermal load.
- For fast transients, there is a cut-off angular frequency for the imposed heat flux beyond which the fluid does not follow the details of the imposed thermal load. The fluid response then becomes that of step heat flux.
- The fluid response consists of two main parts: (i) short-time response and (ii) long-time response. The former is corresponding to early times during which pure conduction occurs inside

the fluid domain. On the other hand, long-time response refers to a period of time starting after the transition time; the fluid yields steady-oscillatory behavior.

- The conventional steady-state models fail to predict the thermal behavior of dynamic cooling systems under time-varying thermal load.

Conflict of interest

None declared.

Acknowledgments

This work was supported by Automotive Partnership Canada (APC), Grant No. APCPJ 401826-10. The authors would like to thank the support of the industry partner, Future Vehicle Technologies Inc. (British Columbia, Canada).

References

[1] M. Marz, A. Schletz, Power electronics system integration for electric and hybrid vehicles, in: 6th Int. Conf. Integr. Power Electron. Syst., 2010, pp. Paper 6.1.
[2] K. Chau, C. Chan, C. Liu, Overview of permanent-magnet brushless drives for electric and hybrid electric vehicles, IEEE Trans. Ind. Electron. 55 (2008) 2246–2257.
[3] J. Garrison, M. Webber, Optimization of an integrated energy storage scheme for a dispatchable wind powered energy system, in: ASME 2012 6th Int. Conf. Energy Sustain. Parts A B San Diego, CA, USA, 2012, pp. 1009–1019.
[4] J. Garrison, M. Webber, An integrated energy storage scheme for a dispatchable solar and wind powered energy system and analysis of dynamic parameters, Renew. Sustain. Energy 3 (2011) 1–11.
[5] C. Crawford, Balance of power: dynamic thermal management for Internet data centers, IEEE Internet Comput. 9 (2005) 42–49.
[6] R.R. Schmidt, E.E. Cruz, M. Iyengar, Challenges of data center thermal management, IBM J. Res. Dev. 49 (2005) 709–723.
[7] Y. Joshi, P. Kumar, B. Sammakia, M. Patterson, Energy Efficient Thermal Management of Data Centers, Springer, US, Boston, MA, 2012.
[8] R. Scott Downing, G. Kojasoy, Single and two-phase pressure drop characteristics in miniature helical channels, Exp. Therm. Fluid Sci. 26 (2002) 535–546.
[9] S.V. Garimella, L. Yeh, T. Persoons, Thermal Management Challenges in Telecommunication Systems and Data Centers Thermal Management Challenges in Telecommunication Systems and Data Centers, CTRC Res. Publ, 2012. pp. 1–26.
[10] M. O'Keefe, K. Bennion, A comparison of hybrid electric vehicle power electronics cooling options, in: Veh. Power Electron. Cool. Options, 2007, pp. 116–123.
[11] C. Mi, F.Z. Peng, K.J. Kelly, M.O'. Keefe, V. Hassani, Topology, design, analysis and thermal management of power electronics for hybrid electric vehicle applications, Int. J. Electr. Hybrid Veh. 1 (2008) 276–294.
[12] R. Siegel, Transient heat transfer for laminar slug flow in ducts, Appl. Mech. 81 (1959) 140–144.
[13] R. Siegel, M. Perlmutter, Laminar heat transfer in a channel with unsteady flow and wall heating varying with position and time, Trans. ASME 85 (1963) 358–365.
[14] R. Siegel, M. Perlmutter, Heat transfer for pulsating laminar duct flow, Heat Transfer 84 (1962) 111–122.
[15] R. Siegel, Heat transfer for laminar flow in ducts with arbitrary time variations in wall temperature, Trans. ASME 27 (1960) 241–249.
[16] M. Perlmutter, R. Siegel, Two-dimensional unsteady incompressible laminar duct flow with a step change in wall temperature, Trans. ASME 83 (1961) 432–440.
[17] M. Perlmutter, R. Siegel, Unsteady laminar flow in a duct with unsteady heat addition, Heat Transfer 83 (1961) 432–439.
[18] R. Siegel, Forced convection in a channel with wall heat capacity and with wall heating variable with axial position and time, Int. J. Heat Mass Transfer 6 (1963) 607–620.
[19] M. Fakoor-Pakdaman, M. Andisheh-Tadbir, M. Bahrami, Transient internal forced convection under arbitrary time-dependent heat flux, in: Proc. ASME Summer Heat Transf. Conf., Minneapolis, MN, USA, 2013.
[20] M. Fakoor-Pakdaman, M. Andisheh-Tadbir, M. Bahrami, Unsteady laminar forced-convective tube flow under dynamic time-dependent heat flux, J. Heat Transfer 136 (2014) 041706.
[21] M. Fakoor-Pakdaman, M. Ahmadi, M. Bahrami, Unsteady internal forced-convective flow under dynamic time-dependent boundary temperature, J. Thermophys. Heat Transfer 28 (2014) 463–473.
[22] M. Fakoor-Pakdaman, M. Ahmadi, M. Andisheh-Tadbir, M. Bahrami, Optimal unsteady convection over a duty cycle for arbitrary unsteady flow under dynamic thermal load, Int. J. Heat Mass Transfer 78 (2014) 1187–1198.
[23] F.P. Incropera, D.P. Dewitt, T.L. Bergman, A.S. Lavine, Introduction to Heat Transfer, fifth ed., John Wiley & Sons, USA, 2007.
[24] Z. Guo, H. Sung, Analysis of the Nusselt number in pulsating pipe flow, Int. J. Heat Mass Transfer 40 (1997) 2486–2489.
[25] A. Bejan, Convection Heat Transfer, third ed., USA, 2004.
[26] M. Fakoor-Pakdaman, M. Bahrami, Transient internal forced convection under step wall heat flux, in: Proc. ASME 2013 Summer Heat Transf. Conf. HT2013, 2013.
[27] T. Von Karman, M.A. Biot, Mathematical Methods in Engineering, McGraw-Hill, New York, 1940.
[28] R.K. Shah, Thermal entry length solutions for the circular tube and parallel plates, in: Proceeding 3rd Natl. Heat Mass Transf. Conf., Indian Institute of Technology, Bombay, 1975, pp. HMT–11–75.
[29] E. Kreyszig, H. Kreyzig, E.J. Norminton, Advanced Engineering Mathematics, 10th ed., John Wiley & Sons, n.d.
[30] S.W. Churchill, R. Usagi, A general expression for the correlation of rates of transfer and other phenomena, Am. Inst. Chem. Eng. 18 (1972) 1121–1128.
[31] R. Siegel, E.M. Sparrow, Transient heat transfer for laminar forced convection in the thermal entrance region of flat ducts, Heat Transfer 81 (1959) 29–36.